Temperature and frequency dependence on dielectric permittivity and electrical conductivity of recycled Liquid Crystals

Ana Barrera, Corinne Binet, Frédéric Dubois, Pierre-Alexandre Hébert, Philippe Supiot, Corinne Foissac, Ulrich Maschke

Temperature and frequency dependence on dielectric permittivity and electrical conductivity of recycled Liquid Crystals

Ana Barrera [a], Corinne Binet [a], Frédéric Dubois [b], Pierre-Alexandre Hébert [c], Philippe Supiot [a], Corinne Foissac [a] and Ulrich Maschke [a,*]

[a] *Unité Matériaux et Transformations (UMET), UMR 8207, CNRS, INRAE, Centrale Lille, Université de Lille, 59000 Lille, France*

[b] *Unité de Dynamique et Structure des Matériaux Moléculaires (UDSMM), UR 4476, Université du Littoral Côte d'Opale, 62100 Calais, France*

[c] *Laboratoire d'Informatique Signal et Image de la Côte d'Opale (LISIC), UR 4491, Université du Littoral Côte d'Opale, 62100 Calais, France*

*Corresponding author: E-mail address: ulrich.maschke@univ-lille.fr

ABSTRACT

The dielectric behavior and the electrical conductivity response of recycled nematic Liquid Crystals (LCs) were studied over a wide range of frequencies (0.1 to 10^6 Hz) and temperatures (100 to -20 °C) with a broadband dielectric spectroscopy technique. These LC mixtures were extracted from a total of 65700 End-Of-Life (EOL)-Liquid Crystals Displays (LCD) such as computers, tablets and TVs of various sizes, brands, and production years. After a stage of purification, the recycled LC blends seemed to possess similar physical properties as conventional nematic LCs. In this report, two types of anchoring of LC molecules, obtained with homeotropic or homogeneous alignment cells, were investigated. All dielectric data were analyzed with adapted models: Havriliak-Negami and Almond West formalisms for the frequency dependence of the data, as well as Arrhenius and Vogel-Fulcher-Tammann models for their temperature dependence. In this article, it is demonstrated that despite the wide variety of EOL-LCD devices used leading to a large number of LC molecules, the frequency and temperature evolution of the recorded spectra are comparable to those of commercial LC mixtures as reported in the literature. Therefore, their future reuse could be envisaged for display applications.

Keywords: nematic liquid crystals; recycling; dielectric properties; modelization.

1. Introduction

The use of Electrical and Electronic Equipment (EEE) is increasingly becoming an indispensable part of modern life [1,2]. A large part of the world population benefits from a higher standard of living, because of their availability, widespread use and simple access [3]. Nevertheless, the way we produce, consume and manage Waste Electrical and Electronic Equipment (WEEE) is not long-term sustainable [4]. The European Directive WEEE (2012/19/EU) has the main objective to reduce the production of WEEE and requires, especially, the disassembly of all Liquid Crystals Displays (LCDs) with an area over 100 cm^2 [5]. These devices may contain hazardous chemicals, which are registered in the European RoHS Directive (2011/65/EU) (Restriction on the use of certain Hazardous Substances) [6].

Since the last half-century, there is grown interest in technologies concerning LCs in all domains of LCD devices. A presence of an average of 5.6 LCD panels per French household was documented in 2018, which is constantly increasing [7]. This growing demand for screens is generating more and more waste as obsolete screens are replaced by newer ones. Excluding premature device replacement, the lifetime of a LCD is approximatively ten years [8]. Televisions, computers and tablets based on LC technologies includes a set of high value-added materials whose recycling represents a strategic issue [9].

Effective recovery of LCD panels is an expensive process that requires sophisticated technologies but revalorization of LCs, one of the main components of LCD panels, could be relevant and profitable. To reuse these End-Of-Life (EOL)-LC mixtures in new devices, they should present similar chemical and physical properties than the original commercial LCs mixtures. For this purpose, purification processes must be established in order to eliminate impurity traces. Indeed, the presence of inorganic impurities in LC mixtures can induce various undesirable effects; for example, they tend to increase the electrical conductivity, which may lead to a loss of electro-optical or optical properties (screen flickering, persistence, long response time…) [10–14].

In the context of this report, the ability of reusing EOL-LC mixtures in new devices will be investigated in terms of their chemical and physical properties. Generally, nematic LCs present two modes of molecular relaxations, which can be observed using dielectric spectroscopy. The first relaxation mode occurs in the frequency range between 10 and 10^6 Hz and is related to the reorientation of the molecular dipoles around the short axis of the LC-molecule. The second relaxation mode, above 1 MHz, is attributed to the reorientation around its long axis [15–17]. In this report, dielectric permittivities and electrical conductivities of recycled LCs have been evaluated and discussed over wide frequency and temperature ranges.

2. Experimental and methods

2.1. Materials

The EOL-LCs studied in this report originate from an electronic waste company located in Northern France named ENVIE^{2}E. LC mixtures were extracted from a heterogeneous deposit of EOL-LCDs including computers, tablets and TVs of different sizes, types, brands and years of production. The average diagonal size of the recovered EOL-LCD was 24 inch. First, EOL-LCDs were manually sorted and dismantled in order to separate different components: electronic boards, batteries, scrap metals, speakers, capacitors, plastic foils, lamps, LCD panels, plastics and plasma glass.

2.2. Separation and Characterization of components

Subsequently, 65700 LCD panels were opened and LCs molecules were extracted using an organic solvent bath. Additional information about the applied LCs extraction process have been developed in a patent filed by U. Maschke *et al*. (2015) [18]. The native extracted solutions consisted mainly of LCs molecules, organic solvent and both organic and inorganic impurities. These solutions have an unusual black coloration that

is not representative of nematic LC molecules meaning that a purification process must be performed.

For this purpose, the extracted EOL-LCs were purified to remove undesirable impurities, using several distillation and chromatographic techniques. Then, the purified LC samples were characterized to determine their optical, thermal and dielectric properties.

After purification, all investigated EOL-LCs exhibited quite comparable dielectric properties at room temperature [19]. Therefore, only one of the obtained LC mixtures named “recycled LC mixture” will be studied as a function of temperature and frequency in the following sections in order to avoid redundancy.

The texture of this LC sample was observed under a Polarizing Optical Microscope (POM) (Olympus BX60), coupled to a Linkam LTS 350 heating/cooling stage with a TMS 94 temperature control unit. POM analysis were carried out in a descending temperature range from 90 to 20 °C. Between 90 and 73 °C, the recycled LC mixture remain**ed** in the isotropic phase where the LCs molecules did not show any order of orientation or position (Fig. 1). The beginning of the isotropic-nematic transition was observed around 73 °C, and thus, the ordered nematic state appears when the temperature decreases and the sample becomes optically opaque. At room temperature, the LC mixture presented a morphology similar to that of nematic LCs (Schlieren texture). To complement the POM study, Differential Scanning Calorimetry (DSC) analysis were performed using a TA Instruments DSC 10 calorimeter at heating and cooling rates of 10°C/min, under continuous nitrogen flow. In the obtained thermogram (Fig. 2), a single glass transition (T_g) was detected around -90 °C. At about 70 °C, an endothermic peak corresponding to the nematic-isotropic transition (T_{NI}) was also identified, and this temperature was in good agreement with that found in the optical analysis. The LC mixture presents thus a large range of temperature of the nematic phase between T_g and T_{NI}.

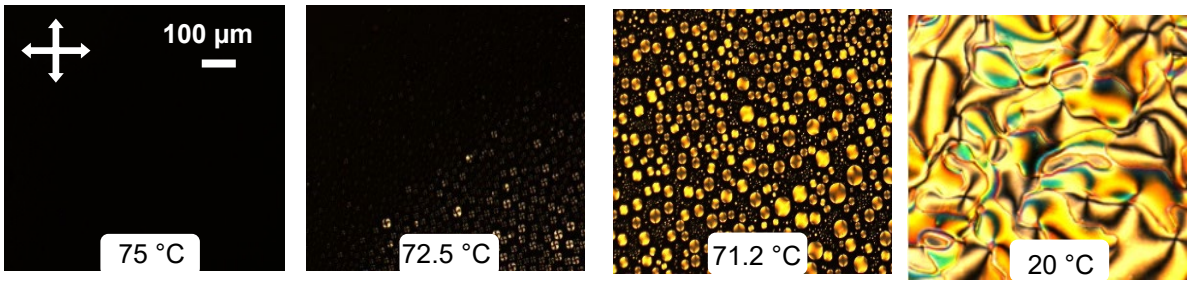

Fig. 1. Texture of the recycled LC mixture observed under Polarizing Optical Microscope (POM) between crossed polarizers in a descending temperature range from 90 to 20 °C. The scale bar represents 100 µm.

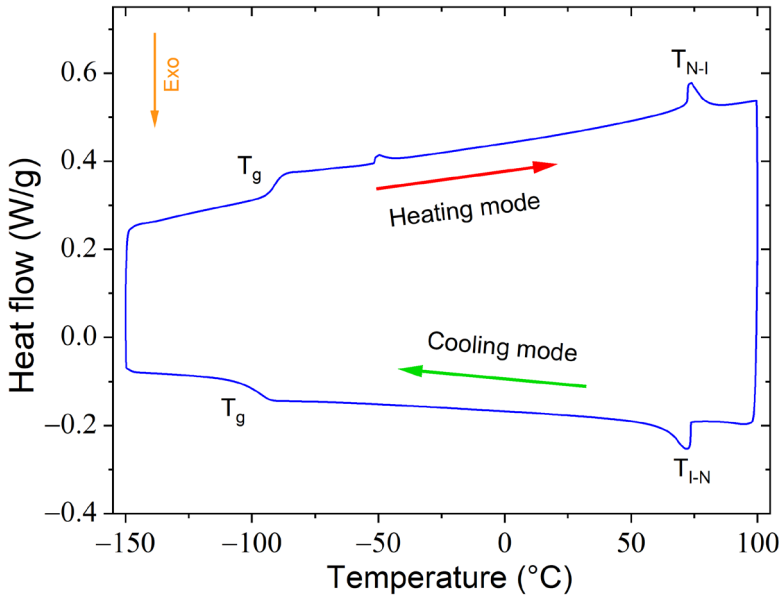

Fig. 2. DSC thermogram of the recycled LC mixture obtained during heating and cooling modes in the temperature range between -150 and 100 °C.

2.2. Dielectric measurements

The Broadband Dielectric Spectroscopy (BDS) measurements were carried out using a ModuLab-MTS impedance analyzer (Solartron Analytical, Ametek) in the frequency range from 0.1 to 10^6 Hz. The amplitude of the applied sine wave voltage was 1 V. The LC samples were inserted into commercial homogeneous (HG) or homeotropic (HT) alignment cells of 20 µm thickness by capillary action at a temperature slightly higher than nematic-isotropic transition (73 °C). The commercial cells used in this study were supplied by AWAT company (Warsaw, Poland). The active surface was 0.25 cm^2 and the sheet resistance of the ITO coating electrode was about 10 Ω/□. The homogeneous and homeotropic alignments of the cells employed in this study were confirmed using

POM, as previously reported by Barrera *et al.* 2021 [19]. The temperature of the samples was controlled with a Linkam LTS350 stage. The temperature range chosen was from 100 to -20 °C.

BDS allows to determinate the complex relative dielectric permittivity ε^*, which can be related to the complex conductivity σ^* by the following relation (Eq. (1)) [20]:

$$\sigma^*(\omega) = i\omega\varepsilon_0\varepsilon^* \quad (1)$$

where ω stands for the angular frequency ($\omega = 2\pi f$, f is the frequency) of the measuring electric field, and ε_0 represents the dielectric permittivity of vacuum (8.85418 ×10^{-12} F.m^{-1}).

The complex relative dielectric permittivity and complex conductivity can be written according to Eqs. (2) and (3):

$$\varepsilon^*(\omega) = \varepsilon'(\omega) - i\varepsilon''(\omega) \quad (2)$$

$$\sigma^*(\omega) = \sigma'(\omega) + i\sigma''(\omega) \quad (3)$$

where ε' and ε'' describe respectively the real part (related to the stored energy) and the imaginary part (related to the dissipated energy) of ε^*; σ' and σ'' represent respectively the real and imaginary parts of σ^*.

To obtain σ' and σ'' from dielectric parameters, Eqs. (4) and (5) are used:

$$\sigma'(\omega) = \omega\varepsilon_0\varepsilon''(\omega) \quad (4)$$

$$\sigma''(\omega) = \omega\varepsilon_0\varepsilon'(\omega) \quad (5)$$

The Almond-West formalism is widely applied to analyze the dependence with frequency of the real part of the complex conductivity. This model is derived from Jonscher's universal power law [21] and can be expressed as follows:

$$\sigma'(\omega) = \sigma_{DC}\left(1 + \left(\frac{f}{f_c}\right)^n\right) \quad (6)$$

where σ_{DC}, f_c and n represent the DC conductivity, the characteristic frequency and the degree of interaction between the mobile ions and their environment, respectively. There are many models allowing to fit the dependence with frequency of the complex conductivity such as the Cole-Cole, Cole-Davidson, Havriliak-Negami (H-N) or Kohl-

Rausch-Williams-Watts equations, previously transformed into their conductivity representation [22–24].

In order to reuse these EOL-LCs in LCD systems, it is also essential to know their dielectric anisotropy ε_a. This parameter characterizes the ability of LC molecules to orient themselves in response to an external electric field. ε_a is obtained from the difference between the dielectric permittivities when the electric field is parallel to the molecular director of the LC called “n” [25] ($\varepsilon'_{//}$ obtained with HT cells) and when the field is perpendicular to “n” ($\varepsilon'_{\perp}$ obtained with HG cells). Therefore, dielectric anisotropy can be expressed by Eq. (7):

$$\varepsilon_a = \varepsilon'_{//} - \varepsilon'_{\perp} \quad (7)$$

3. Results and discussion

3.1 Temperature dependence of dielectric permittivity and electrical conductivity of the recycled LC mixture

3.1.1 Dielectric permittivity spectra

The evolution with temperature and frequency of the real and imaginary parts of ε^* of the recycled LC mixture in HT and HG alignments is presented in Fig. 3 and 4. The temperature range chosen is comprised between 100 °C and -20 °C, and the results are presented in cooling mode. These temperatures were selected in relationship with those used for industrial LCD applications.

In HT alignment, the dielectric spectra ε'(f) depend strongly on both temperature and frequency (Fig. 3 a). At high temperatures and a frequency of 0.1 Hz, ε' reaches its highest value of 650 whereas at low temperatures ε' decreases to around 10. The significant increase of ε' with decreasing frequency is due to a phenomenon of polarization of charges and the contribution of the electrical conductivity [20,26]. When the temperature decreases, both phenomena are shifted towards low frequencies. At intermediate and high frequencies, ε' show**s** a frequency independent plateau for

temperatures from 100 to 75 °C. Below 70 °C in the frequency region about 10^5 Hz, ε' starts to decrease slightly due to the appearance of relaxation mechanisms.

Fig. 3 b) shows the ε''(f) spectra of the recycled LC mixture in HT alignment. At low frequencies, the increase of ε'' with decreasing frequency can be attributed to phenomena of conduction and electrode polarization. For temperatures below 20 °C and in the frequency range between 10^2 and 10^6 Hz, two overlapping dielectric relaxation mechanisms can be observed. With decreasing sample temperature, these mechanisms shift to the intermediate frequency region. The main mechanism, although of lower amplitude, is located between ~10^2 and 10^3 Hz and probably related to the dielectric LC glass transition (around -90 °C). The secondary mechanism, localized between ~10^4 and 10^6 Hz, is attributed to the process of rotation/reorientation of LC molecules around their minor axis [17,27,28]. This phenomenon could also be related to the contribution of parasitic impedances caused by connectors, cables, etc., which become significant at frequencies above 100 kHz [19] [26], and the relaxation of the measuring cell due to the resistance of the ITO layer [29–31]. However, these parasitic effects and ITO influences seem to be absent here since the empty cell dielectric measurements in both alignments at different temperatures did not reveal such effects in the frequency window of the experiment.

Following current literature, the dielectric relaxation mechanisms were analyzed by applying known models (Debye, Cole-Cole, Cole-Davidson and Havriliak-Negami) [22–24,32]. The study of these mechanisms will be presented in the following section.

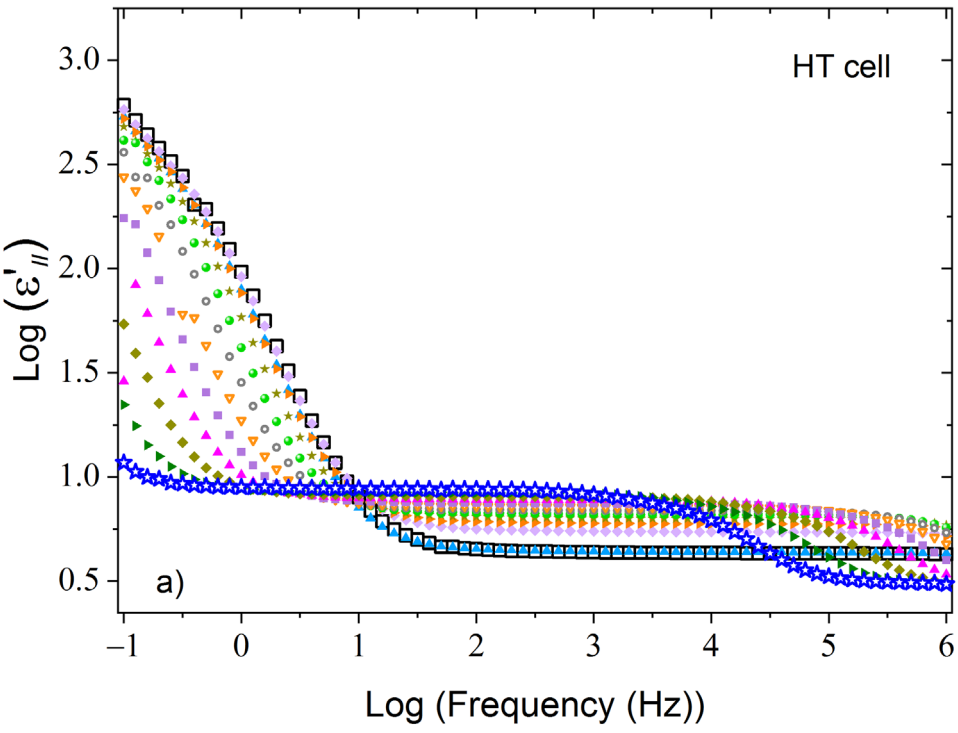

206

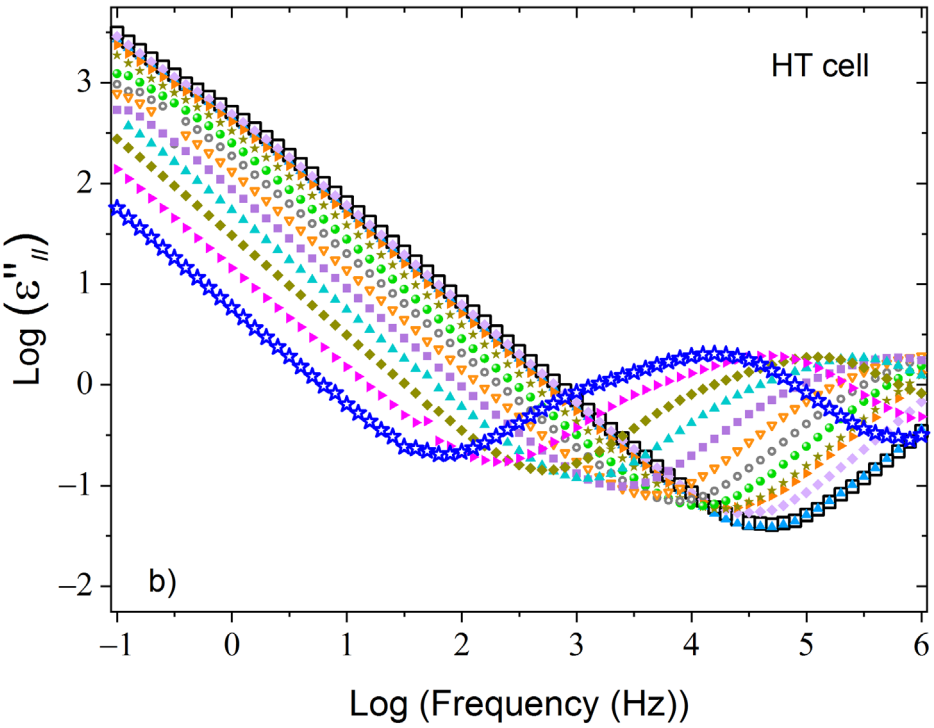

207

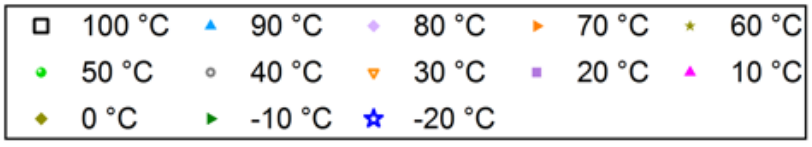

208

Fig. 3. Dielectric spectra a) ε'(f) and b) ε''(f) of the recycled LC mixture in homeotropic alignment. The spectra were taken in a descending temperature range between 100 and -20 °C. 209 210 211

The dielectric spectra ε'(f) and ε''(f) of the recycled LC mixture in HG alignment are presented in Fig. 4 a) and 4 b), respectively. The behaviors are very similar to those observed in HT alignment. However, conduction and interfacial polarization phenomena appear at slightly higher frequencies for all considered temperatures. Furthermore, the amplitudes of the relaxations observed at high frequency and low temperature seem to be slightly less intense than in the HT alignment.

It is interesting to note that the evolutions with frequency and temperature of the spectra observed for the recycled LC mixture are comparable to those of commercial LC mixtures reported in the literature [27,28].

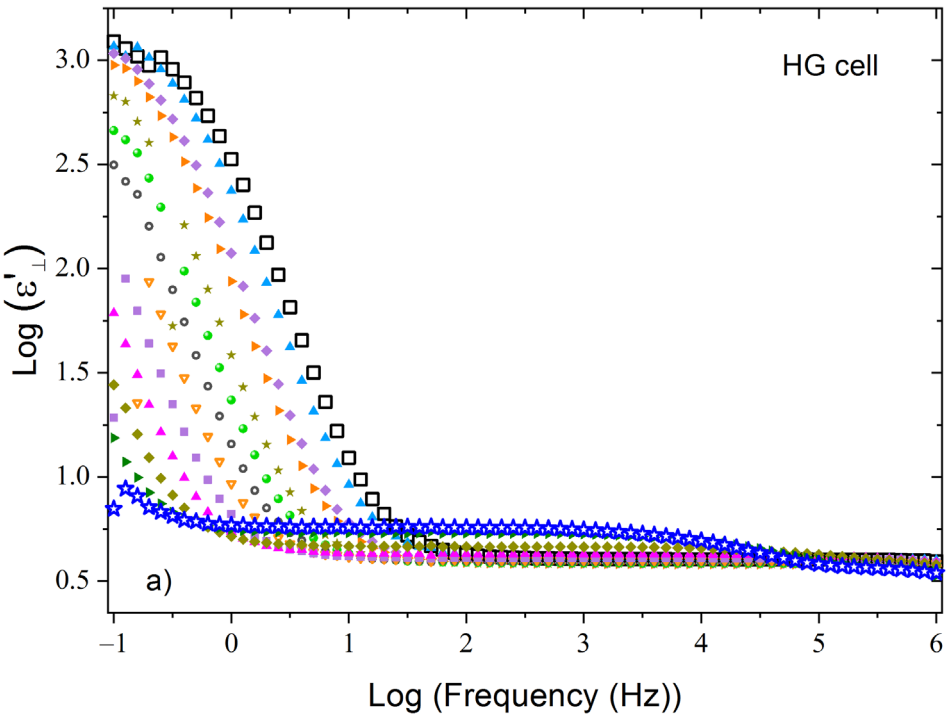

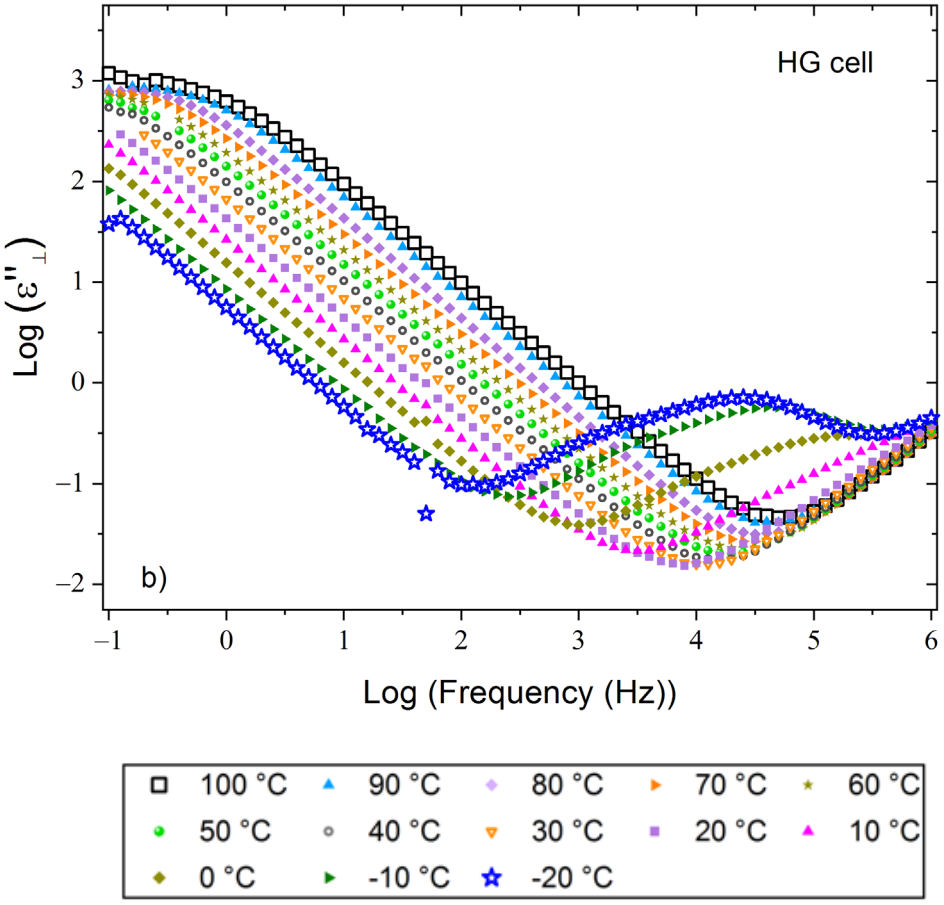

Fig. 4. Dielectric spectra a) ε'(f) and b) ε''(f) of the recycled LC mixture in homogeneous alignment. The spectra were taken in a descending temperature range between 100 and -20 °C.

3.2 Dielectric relaxation mechanisms

3.2.1 Havriliak-Negami model

The dielectric relaxation mechanisms were studied applying the H-N formalism. In order to perform an analysis of the experimental data in the whole frequency range, a supplementary term was added to the original formalism. The modified H-N model is illustrated in Eq. (8):

$$\varepsilon^*(f) = \varepsilon_\infty + \sum_k \frac{\Delta\varepsilon_k}{\left[1+\left(i\frac{f}{f_{ck}}\right)^{\alpha_k}\right]^{\beta_k}} + \frac{\sigma}{\varepsilon_0(i2\pi f)^n} \quad (8)$$

where k indexes the relaxation mechanisms, $\Delta\varepsilon$ is the strength of the relaxation mechanism and represents the decrease of the real part of the complex dielectric permittivity ($\Delta\varepsilon = \varepsilon_s - \varepsilon_\infty$ with ε_s and ε_∞ being the low (static) and high frequency

permittivities, respectively). f_c corresponds to the characteristic frequency also called relaxation frequency, and α and β are the shape parameters describing the width and asymmetry of the dielectric spectra, respectively ($0 < \alpha, \beta \leq 1$). The added term corresponds to the contribution of the electrical conductivity; ε_0 represents the vacuum permittivity, σ is associated with the DC conductivity, and n stands for the degree of interaction between the mobile ions and their environment.

The spectra $\varepsilon'(f)$ and $\varepsilon''(f)$ were simultaneously fitted with Eq. (8) using the Levenberg-Marquardt algorithm, applying Grafity software. Fig. 5 a) shows the fit of the dielectric spectra $\varepsilon'(f)$ and $\varepsilon''(f)$ of the recycled LC mixture at -20 °C in HT alignment. The experimental data and the fit are represented by symbols and red solid lines, respectively. Fig. 5 b) shows the decomposition of the fit of the $\varepsilon''(f)$ spectrum into three processes: the contribution of the electrical conductivity (black line at low frequencies) and two H-N relaxations (the main relaxation in blue color at intermediate frequencies and the secondary one in green color at high frequencies). The inset of this figure shows the secondary mechanism on a linear y-scale to highlight the quality of the fit.

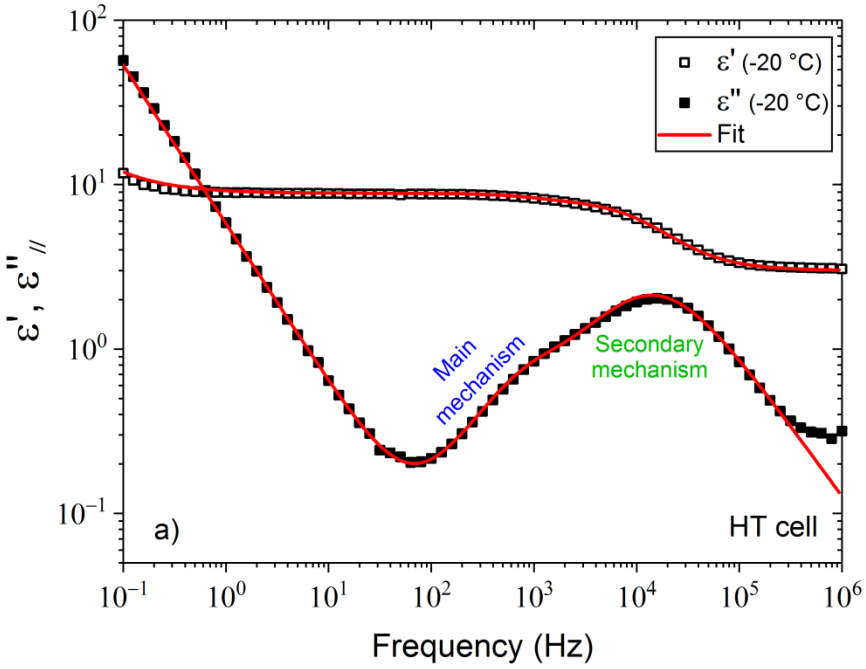

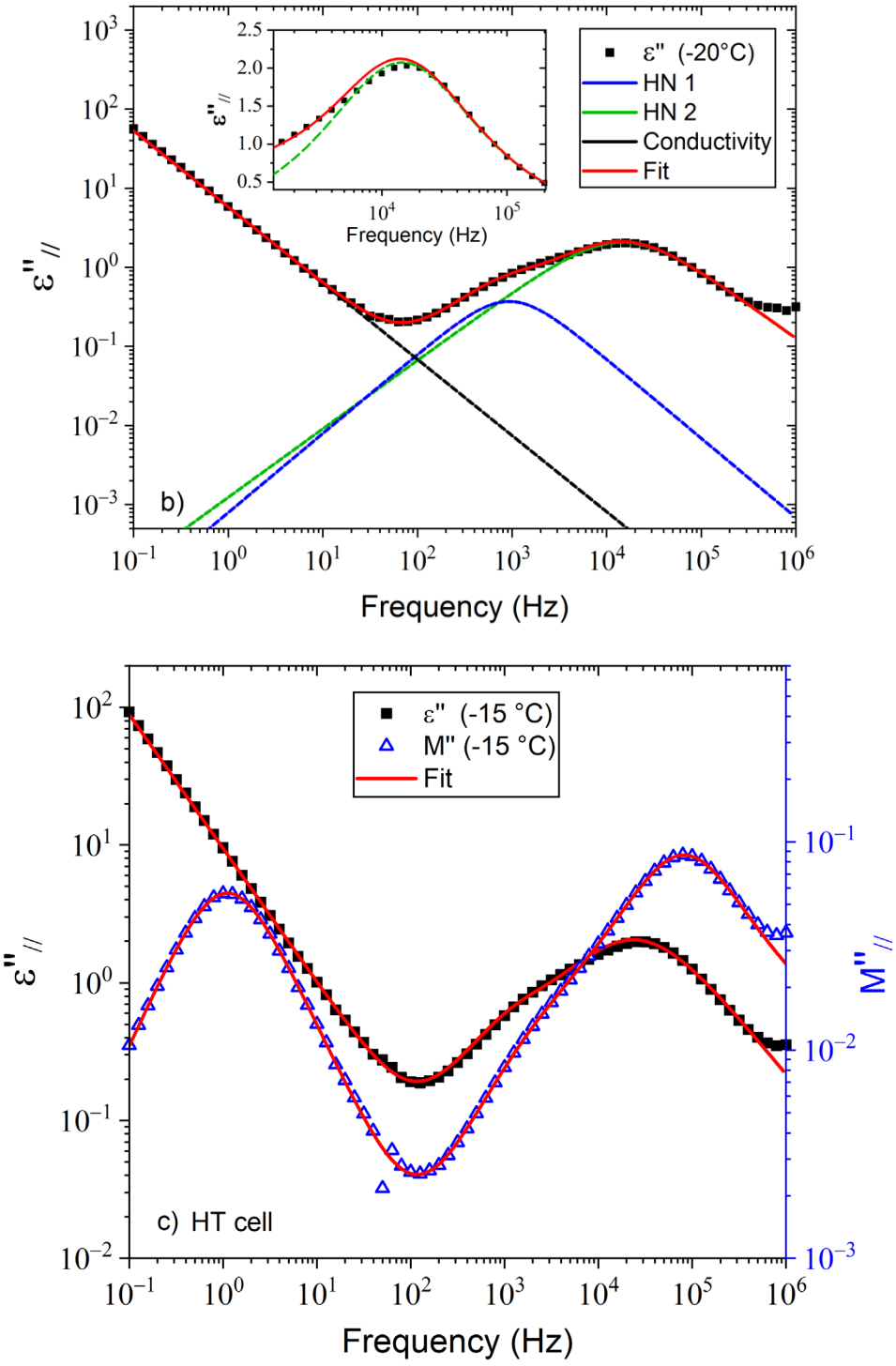

Fig. 5. a) Simultaneous fit to the H-N model of the dielectric spectra $\varepsilon'(f)$ and $\varepsilon''(f)$ of the recycled LC mixture at -20 °C in HT alignment; the fit is represented by the red solid line. b) Decomposition of the dielectric spectrum $\varepsilon''(f)$ into three processes: two relaxation mechanisms and electrical conductivity. The inset represents the secondary mechanism using a linear y-scale. c) Example of dielectric spectra $\varepsilon''(f)$ and $M''(f)$ at -15 °C in HT alignment.

Table 1 reports the fit parameters obtained using the H-N model for the recycled LC mixture in HT alignment from -20 to 15 °C and in HG alignment from -20 to 0 °C. Outside these temperature ranges, the dielectric strength of the main mechanism is insufficient within the studied frequency window, and the characteristic frequency of the secondary mechanism is too high to allow fitting.

The main relaxation mechanism of the LC mixture in both alignments exhibits Cole-Cole behavior at -20 °C and follows the Debye model for all other temperatures. The Cole-Cole equation can also be used to fit the secondary relaxation mechanism, except when the LC is in HG alignment at 0 °C; in this case the H-N formalism is required. As the temperature decreases, and thus approaches T_g, the characteristic frequency of the mechanisms decreases and their dielectric strength increases. The evolution with temperature of the characteristic frequency is detailed in the next section.

Table 1. H-N model parameters for fitting dielectric spectra $\varepsilon'(f)$ and $\varepsilon''(f)$ of the recycled LC mixture in HT and HG alignments.

				Main mechanism				Secondary mechanism			
T (°C)	σ (nS.m^{-1})	n	f_{c1} (kHz)	$\Delta\varepsilon_1$	α	β	f_{c2} (kHz)	$\Delta\varepsilon_2$	α	β	R^2
HT cell											
15	3.82	0.98	39.81	0.15	1	1	414.3	4.16	0.794	1	0.995
10	2.92	0.98	23.12	0.31	1	1	269.1	4.96	0.819	1	0.995
5	2.37	1.00	14.04	0.16	1	1	174.3	5.41	0.776	1	0.996
0	1.86	1.00	7.786	0.13	1	1	108.0	5.45	0.762	1	0.997
-5	1.06	0.97	5.002	0.53	1	1	69.46	4.95	0.846	1	0.999
-10	0.739	0.97	3.135	0.55	1	1	42.88	5.05	0.842	1	0.998
-15	0.498	0.97	1.460	0.55	1	1	24.32	5.19	0.841	1	0.999
-20	0.301	0.96	0.931	0.74	0.949	1	14.50	5.32	0.867	1	0.998
HG cell											
0	0.863	1.00	---	---	---	---	288.4	1.21	0.629	1	0.987
-5	0.762	0.99	3.990	0.03	1	1	92.63	1.42	0.667	1	0.989
-10	0.474	0.98	2.769	0.11	1	1	43.57	1.72	0.749	1	0.998
-15	0.411	0.99	1.441	0.17	1	1	22.55	2.44	0.773	1	0.999
-20	0.318	1.00	1.065	0.19	0.966	1	13.40	2.55	0.737	1	0.999
Uncertainty (%)	1-5	0.5-4	4-8	3-10	2-5	2-5	5-8	2-10	1-4	2-5	

To complement the obtained results from the dielectric formalism, the complex dielectric modulus ($M^* = 1/\varepsilon^*$) has been employed. This representation could provide a more complete picture of the system and the imaginary part (M'') of M^* offers information in terms of conductivity. An example of M'' as a function of frequency, taken at -15 °C, is shown in Fig. 5 c). Complementary results are presented in supplementary part (Fig. S1). Fig. 5 c) exhibits a Debye peak appearing at low frequencies associated to the conductivity. Two other relaxations peaks, linked to main and secondary modes, were also found. Analysis of all data allowed to follow the frequency evolution of the peak maxima (f_{max}) as a function of temperature (see next section).

3.2.2 Dependence of the characteristic frequency on temperature

The Arrhenius (Eq. (9)) and the Vogel-Fulcher-Tammann laws (VFT) (Eq. (10)) are commonly used to analyze the Arrhenius plot of the characteristic frequency of relaxation mechanisms.

$$f_c = f_{c0}\, exp\left(-\frac{E_a}{kT}\right) \quad (9)$$

where f_{c0} is the pre-exponential factor, E_a represents the activation energy, k stands for the Boltzmann constant (1.38×10^{-23} J·K^{-1}) and T is the temperature in Kelvin.

$$f_c = f_{c0}\, exp\left(-\frac{B}{T-T_0}\right) \quad (10)$$

where B represents the "pseudo activation energy" $\left(B = \frac{E_a}{k}\right)$ in Kelvin and T_0 is known as the Vogel temperature. T_0 is always 30 to 70 °C lower than T_g.

The Arrhenius plot of the characteristic frequency of the main and secondary relaxation mechanisms of the recycled LC mixture in HT alignment is shown in Fig. 6 as well as obtained results from M'' analysis. It can be seen that both mechanisms exhibit Arrhenius-like behavior. The activation energies obtained by fitting the experimental data (Eq. (9)) are gathered in Table 2.

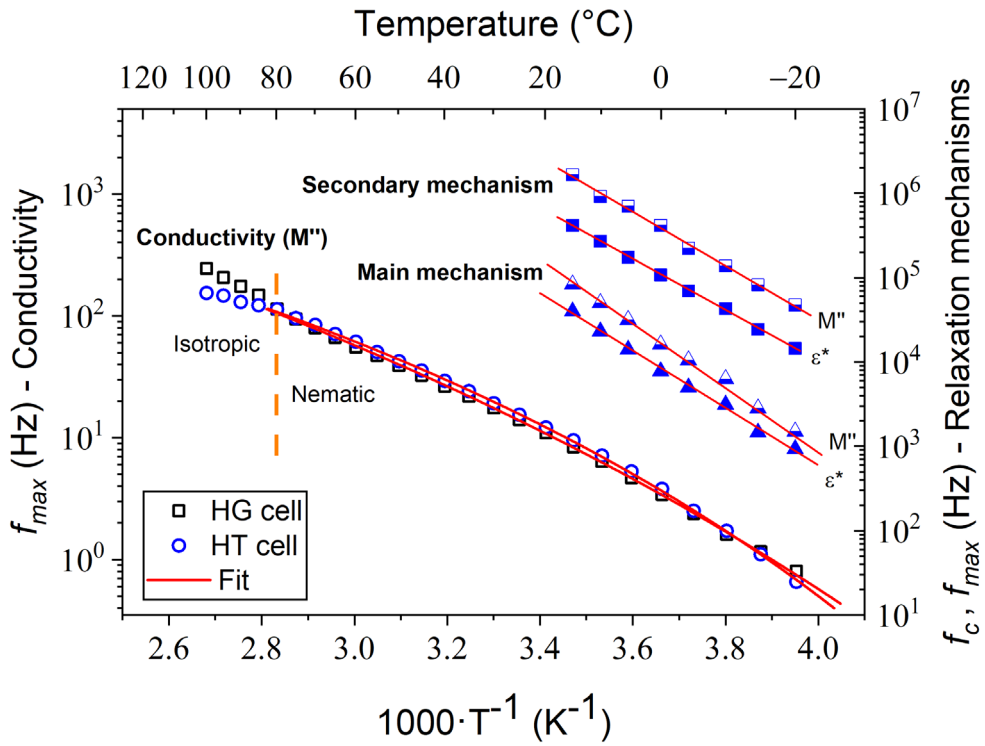

Fig. 6. Arrhenius plot of characteristic frequencies and frequency evolution of the peak maxima of the mechanisms for recycled LC mixture in HT alignment obtained from ε^* and M''. The experimental data and the fits to the Arrhenius model are represented by symbols and red solid lines, respectively. Results from HG cell are presented only for conductivity data from M''.

Table 2. Arrhenius activation energy of the relaxation mechanisms of the recycled LC mixture in HT and HG alignments (fit for HG alignment is given in supplementary material, Fig. S2).

		Main mechanism	Secondary mechanism
		E_a (eV)	E_a (eV)
HT cell	ε''	0.684 ± 0.003	0.602 ± 0.003
	M''	0.734 ± 0.002	0.645 ± 0.001
HG cell	ε''	0.541 ± 0.050	0.741 ± 0.052
	M''	0.794 ± 0.054	0.657 ± 0.064

The main mechanism, previously associated with T_g, was expected to exhibit VFT behavior. Nevertheless, the experimental data follow the Arrhenius model; this may be related to the fact that the narrow temperature range investigated for the dielectric

study is far from T_g ~ -90 °C. The secondary mechanism also follows an Arrhenius-like behavior, as reported by other authors; it is associated to the molecular rotation around the minor axis [17]. The activation energies obtained are consistent with the values found in the literature for commercial nematic LC mixtures [17,27,33]. Fig. 6 also exhibits frequency data from the peak maxima of M''. These values, for the main and secondary mechanisms, were found to be higher than the characteristic frequencies from ε^*. As expected, almost parallel lines have been observed in Fig. 6 as function of the reduced temperature ($1000 \cdot T^{-1}$). Indeed, f_c and f_{max} are proportional and associated by $f_{max} = \left(\frac{\varepsilon_s}{\varepsilon_\infty}\right) fc$ [26]. It should be mentioned that the latter equation is only valid in the case of Debye-like relaxation. The obtained activation energies (Table 2) are comparable since the same relaxation mechanisms are involved. Considering the results of the maxima deduced from conductivity peak of M'' in both alignments, a VFT-like behavior was observed. The corresponding T_0 values were 129 and 154 K for HG and HT alignments, respectively, thus in good agreement with the T_g (183 K) value determined by DSC analysis.

3.3 Dielectric anisotropy

Fig. 7 shows the evolution with the inverse of the temperature of the real part of the complex dielectric permittivity of the recycled LC mixture, and of its dielectric anisotropy ε_a determined at 1 kHz. At high temperatures, when the LC mixture is in the isotropic phase, the perpendicularly and parallel permittivities are very close, consequently ε_a is very small. As the temperature decreases, in the nematic phase, the permittivity of the LC mixture in HG alignment changes little ($\varepsilon'_{\perp} \sim 4.0$), whereas that in HT alignment increases steadily up to T= -5°C. The latter behavior is due to the decrease in dynamic/thermal movements of the molecules as the temperature decreases [34]. From -5 °C to -20°C, the permittivity of the LC mixture in HT alignment varies little ($\varepsilon'_{//} \sim 8.2$). Thus, the dielectric anisotropy shows a similar evolution as that

of the longitudinal component $\varepsilon'_{//}$ of the permittivity, and reaches a value of 4.0 at T= -5°C.

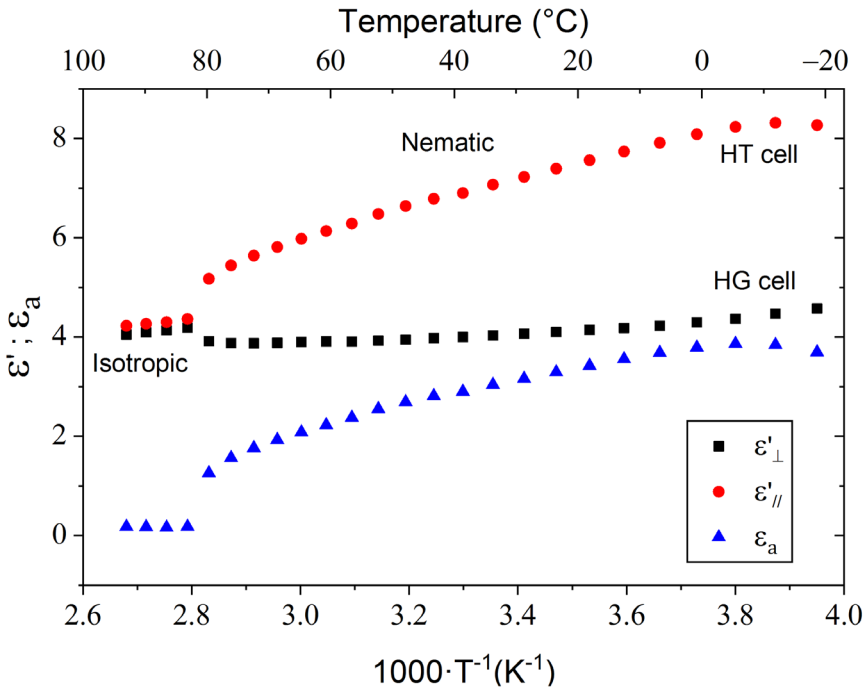

Fig. 7. Evolution with the inverse temperature of the real part of the complex dielectric permittivity of the recycled LC mixture, and of the dielectric anisotropy (temperature (°C) as secondary X axis).

3.4 Electrical conductivity spectra

Figures 8 a) and b) show the dependence with temperature of the real part of the complex conductivity of the recycled LC mixture in HT and HG alignments respectively, and the fits of these spectra to the Almond-West model (Eq. (6)). For reasons of clarity, only a few temperatures were illustrated. Nevertheless, spectra over the entire temperature range were presented in the supplementary material (Fig. S3). When the recycled LC mixture is in HT alignment, two behaviors can be distinguished (Fig. 8 a):

- At low frequencies, a plateau corresponding to the DC conductivity is observed. Conductivity values increase with temperature. This behavior suggests that electrical conductivity in LCs represents a thermally activated process [26]. At very low frequencies (<1 Hz), and temperatures between 100 and 20 °C, the σ' values of the mixture decrease as the frequency decreases, due to the electrode polarization. This effect will not be taken into account in this report.

- At higher frequencies, conductivity depends on frequency and increases drastically with it. This is due to the ionic relaxation of mobile charge carriers. This effect is known as subdiffusive conductivity. Between 10 kHz and 1 MHz, a weak decrease in σ' appears from 20 to -20 °C due to the relaxation mechanisms already observed in the dielectric spectra (Fig. 3 a and b). These observations are also valid when the LC alignment is homogeneous (Fig. 8 b). However, in this configuration, at low frequencies, the phenomenon of polarization of the electrode seems more important and visible.

The evolution with temperature (100 to -20°C) of the DC conductivity of the recycled LC mixture in HT and HG alignments is analyzed in the following section using the Almond-West formalism.

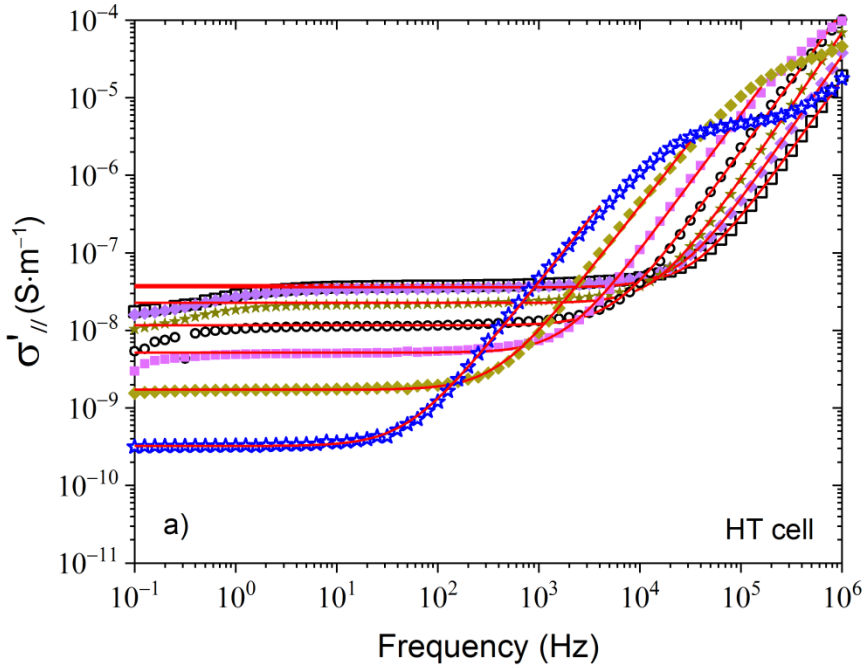

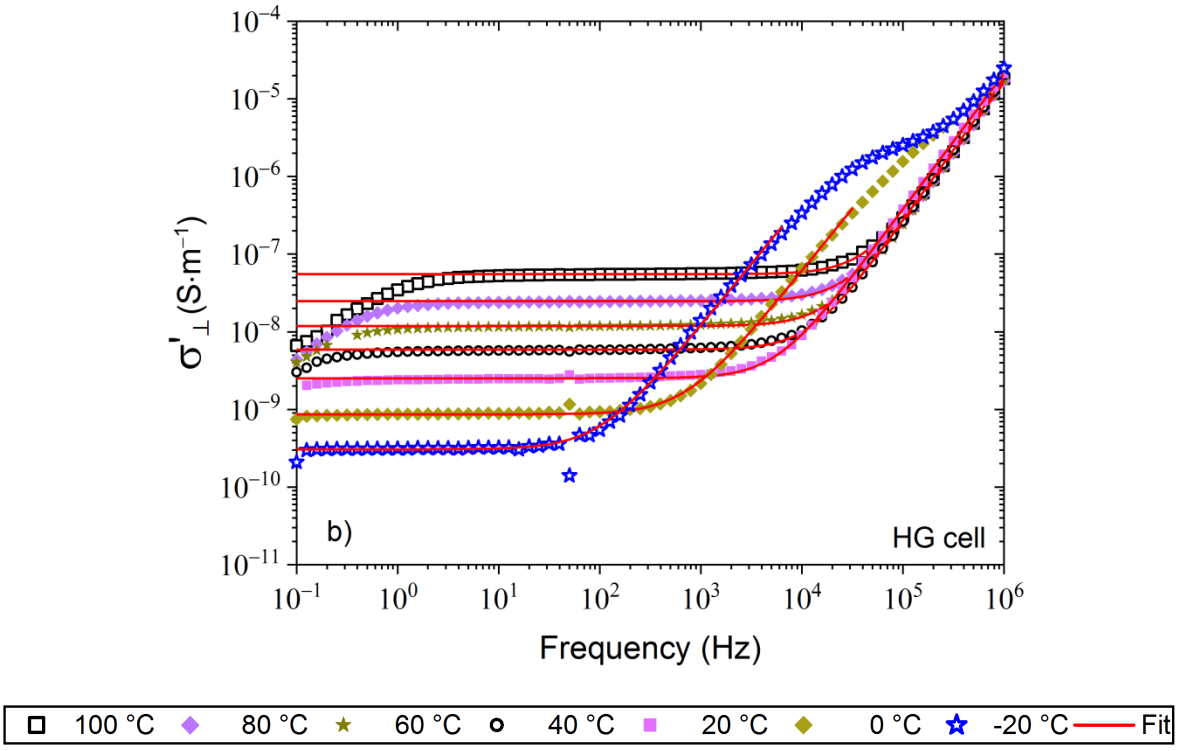

Fig. 8. Conductivity spectra σ'(f) of the recycled LC mixture in a) HT and b) HG alignments from 100 to -20 °C. The experimental data and the fits to the Almond-West model are represented by symbols and red solid lines, respectively.

3.5 DC conductivity

The Arrhenius plot of the DC conductivity obtained with Eq. (6) are analyzed with the Arrhenius and VFT models given by Eqs. (11) and (12), respectively [17,26].

$$\sigma_{DC} = \sigma_{DC0}\, exp\left(-\frac{E_a}{kT}\right) \quad (11)$$

$$\sigma_{DC} = \sigma_{DC0}\, exp\left(-\frac{B}{T-T_0}\right) \quad (12)$$

where σ_{DC0} is a pre-exponential factor. The other parameters have already been presented in section 3.2.2. The Arrhenius plot of the DC conductivity for the two LC alignments and the fits to the VFT and Arrhenius models in the nematic phase are shown in Fig. 9 for the recycled LC mixture.

The plot in HT alignment follows the VFT model. In contrast, the plot in HG alignment cannot be correctly fitted using either Arrhenius or VFT models over the entire temperature range (supplementary material, Fig. S4). In particular, the use of the VFT

model leads to an uncertainty on the results of more than 20% (Table 3). In fact, the combination of the Arrhenius formalism from 80 to 10 °C and the VFT model from 10 to -20 °C allows a better fit of the activation plot of the DC conductivity of the recycled LC mixture (Fig. 9, Table 3). VFT-like behavior was expected for the recycled LC mixture in both alignments. If we exclude the approach, the device and the types of cells used, it is obvious that the mixtures of purified LCs are responsible for this behavior. Several hypotheses can explain this behavior:

- The nature and quantity of the LC molecules and ionic species of the recycled mixture are not exactly known.
- Chemical, thermal and optical characterizations have proved that these mixtures present macroscopically an eutectic behavior with very similar characteristics. However, their behavior at the microscopic scale is not known.
- Some LC molecules and ions present in the mixture may act preferentially on the HG or HT alignment of the cell. In addition, the proportion of molecules/ions that interact may be different for each alignment.

The Arrhenius activation energy of DC conductivity of the recycled LC mixture from 80 to 10 °C is equal to 0.341 eV, which is in good agreement with the data from literature for commercial nematic LCs [17,27,33]. Moreover, the value of the Vogel temperature of this mixture (T_g = 166 K) is consistent with the glass transition temperature determined by DSC method (T_g = 183 K), as already mentioned before (cf. data from M''). The DC conductivity values obtained with the Almond-West formalism and by Eq. (8) are in complete agreement.

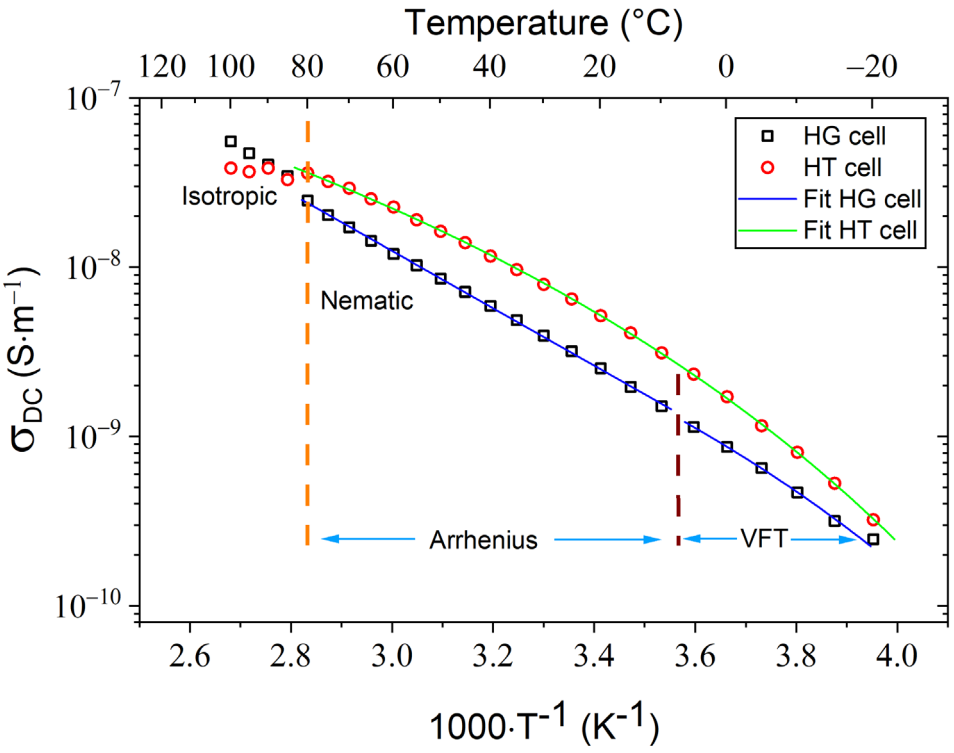

Fig. 9. Arrhenius plot of the DC conductivity of the recycled LC mixture in HT and HG alignments (temperature in °C as secondary X axis). The experimental data and the fits to VFT and Arrhenius models in nematic phase are represented by symbols and solid lines, respectively.

Table 3. Arrhenius and VFT models parameters for fitting Arrhenius plots of the DC conductivity of the recycled LC mixture in HT and HG alignments (Conductivity spectra).

	HG cell				
	E_a (eV)	$\sigma_{DC0\ Arr}$ (S·m^{-1})	B (K)	T_0 (K)	$\sigma_{DC0\ VFT}$ (S·m^{-1})
Arrhenius	0.341 ± 0.001	2.7E-03 ± 1.1E-05	---	---	
VFT	---	---	2189 ± 489	59 ± 17	6.9E-05 ± 8.2E-06
Arrhenius + VFT	0.336 ± 0.001	2.1E-03 ± 1.2E-05	642 ± 7	166 ± 5	3.5E-07 ± 1.2E-09
	HT cell				
VFT	---	---	779 ± 9	165 ± 3	2.3E-06 ± 2.1E-07

4. Conclusions

In this report, the dielectric properties of a recycled LC mixture were studied using an impedance analyzer in the frequency range between 0.1 and 10^6 Hz, and in both homogeneous and homeotropic alignments. Measurements were limited to the

temperature range from 100 to -20 °C in which an LCD device is typically used according to the technical specifications. Furthermore, this range covered the nematic and isotropic phases of the investigated EOL-LCs. It has been illustrated that the frequency and temperature evolutions of the obtained spectra are conveniently comparable with those of conventional LC mixtures reported in literature. Two overlapping dielectric relaxation mechanisms were observed at temperatures below 20 °C and in the frequency range located between 10^2 and 10^6 Hz for both alignments. These phenomena, named main and secondary mechanisms, were attributed to the dielectric LC glass transition (T_g = -90 °C, determined by DSC analysis), and the rotation of LC molecules around the short axis, respectively, and they follow an Arrhenius-like behavior. In contrast, the Arrhenius plot of the DC conductivity do not follow the same model in both alignments. These results revealed that the charge transport phenomena in both homogeneous and homeotropic alignments are not governed by the same mechanisms. Finally, the Arrhenius activation energies of the relaxation mechanisms as well as the DC conductivity of the recycled LC mixture are in good agreement with those of commercial nematic LCs as documented in literature. Regardless of the diverse EOL-LCDs devices collected at the company, it was possible to obtain recycled LC mixtures with thermal, optical, dielectric and electric properties equivalent to those of conventional LCs mixtures. Therefore, their future reuse could be envisaged for display applications.

CRediT authorship contribution statement

Ana Barrera: Conceptualization, Methodology, Investigation, Data curation, Writing—original draft preparation, **Ulrich Maschke:** Conceptualization, Writing—original draft preparation, **Corinne Binet:** Methodology, Investigation, Data curation, **Corinne Foissac:** Writing—review and editing, **Philippe Supiot:** Writing—review and editing, **Frédéric Dubois:** Methodology, software and data validation, **Pierre-Alexandre Hébert:** Software and data validation. All authors have read and agreed to the published version of the manuscript.

Declaration of Competing Interest

The authors declare that they have no known competing financial interests or personal relationships that could have appeared to influence the work reported in this paper.

Acknowledgments

The authors acknowledge financial support from the University of Lille, the “Région Hauts-de-France (FEDER)”, I-Site of Lille and ENVIE^{2}E du Nord.

Funding

This work was supported by Région Hauts-de-France (FEDER), I-Site Lille and ENVIE^{2}E du Nord.

Appendix A. Supplementary material

The following are the Supplementary data to this article:

References

[1] V. Goodship, A. Stevels, J. Huisman, Waste electrical and electronic equipment (WEEE) Handbook, 2 nd ed., Woodhead Publishing (Elsevier), Cambridge, UK, 2019. https://doi.org/10.1016/C2016-0-03853-6.

[2] O.S. Shittu, I.D. Williams, P.J. Shaw, Global E-waste management: Can WEEE make a difference? A review of e-waste trends, legislation, contemporary issues and future challenges, Waste Manag. 120 (2021) 549–563. https://doi.org/10.1016/j.wasman.2020.10.016.

[3] C.P. Baldé, E. D’Angelo, V. Luda, O. Deubzer, R. Kuehr, Global Transboundary E-waste Flows Monitor 2022, United Nations Institute for Training and Research, Bonn, Germany, 2022.

[4] V. Forti, C.P. Baldé, R. Kuehr, G. Bel, The Global E-waste Monitor 2020: Quantities, flows and the circular economy potential., United Nations University (UNU)/United Nations Institute for Training and Research (UNITAR), Bonn-Geneva-Rotterdam, 2020.

[5] European Union, WEEE Directive 2012/19/EU, (2012). https://eur-

lex.europa.eu/legal-content/EN/TXT/?uri=uriserv%3AOJ.L_.2012.197.01.0038.01.ENG&toc=OJ%3AL%3A2012%3A197%3ATOC (accessed November 17, 2022).

[6] European Union, Restrictions on the use of certain hazardous substances in electrical and electronic equipment, (2017). https://eur-lex.europa.eu/summary/EN/uriserv%3A2004_4 (accessed November 17, 2022).

[7] Conseil supérieur de l'audiovisuel, L'équipement audiovisuel des foyers au 1er semestre 2018, (2018). https://www.csa.fr/Informer/Collections-du-CSA/Panorama-Toutes-les-etudes-liees-a-l-ecosysteme-audiovisuel/Les-observatoires-de-l-equipement-audiovisuel/L-equipement-audiovisuel-des-foyers-au-1er-semestre-2018 (accessed November 17, 2022).

[8] A. Amato, F. Beolchini, End of life liquid crystal displays recycling: A patent review, J. Environ. Manage. 225 (2018) 1–9. https://doi.org/10.1016/j.jenvman.2018.07.035.

[9] A. Akcil, I. Agcasulu, B. Swain, Valorization of waste LCD and recovery of critical raw material for circular economy: A review, Resour. Conserv. Recycl. 149 (2019) 622–637. https://doi.org/10.1016/j.resconrec.2019.06.031.

[10] R. Basu, Soft memory in a ferroelectric nanoparticle-doped liquid crystal, Phys. Rev. E - Stat. Nonlinear, Soft Matter Phys. 89 (2014) 1–5. https://doi.org/10.1103/PhysRevE.89.022508.

[11] Y. Garbovskiy, I. Glushchenko, Nano-objects and ions in liquid crystals: Ion trapping effect and related phenomena, Crystals. 5 (2015) 501–533. https://doi.org/10.3390/cryst5040501.

[12] A. Kumar, D. Varshney, J. Prakash, Role of ionic contribution in dielectric behaviour of a nematic liquid crystal with variable cell thickness, J. Mol. Liq. 303 (2020). https://doi.org/10.1016/j.molliq.2020.112520.

[13] O. V. Kovalchuk, T.M. Kovalchuk, N. Tomašovičová, M. Timko, K. Zakutanska, D. Miakota, P. Kopčanský, O.F. Shevchuk, Y. Garbovskiy, Dielectric and electrical properties of nematic liquid crystals 6CB doped with iron oxide nanoparticles. The combined effect of nanodopant concentration and cell thickness, J. Mol. Liq. 366 (2022). https://doi.org/10.1016/j.molliq.2022.120305.

[14] K. Neyts, F. Beunis, Ion transport in liquid crystals, in: J.W. Goodby, C. Tschierske, P. Raynes, H. Gleeson, T. Kato, P.J. Collings (Eds.), Handb. Liq. Cryst., 2nd ed., Wiley-VCH Verlag GmbH & Co. KGaA., Weinheim, Germany, 2014: pp. 1–26.

[15] M. Mrukiewicz, P. Perkowski, K. Garbat, R. Dąbrowski, Molecular relaxations in dual-frequency nematic liquid crystals, Liq. Cryst. 41 (2014) 1537–1544. https://doi.org/10.1080/02678292.2014.932451.

[16] M. Bourg, M. Urbanski, Spectroscopic insight into molecular fluctuations and phase stability of nematic composites containing gold nanoparticles or carbon nanotubes, Phys. Chem. Chem. Phys. 19 (2017) 23302–23308. https://doi.org/10.1039/c7cp02943h.

[17] R. de la Fuente, D. Dunmur, Dielectric properties of liquid crystals, in: J.W. Goodby, C. Tschierske, P. Raynes, H. Gleeson, T. Kato, P.J. Collings (Eds.), Handb. Liq. Cryst., 2 nd ed, Wiley-VCH Verlag GmbH & Co. KGaA.: Weinheim, Germany, Weinheim, Germany, 2014: pp. 1–10. https://doi.org/10.1051/anphys/197803030197.

[18] U. Maschke, I. Moundoungou, G.J. Fossi-Tabieguia, Method for extracting the liquid crystals contained in an element that comprises a first support and a second support - associated device, FR3017808 (A1), EP3111276 (A1), WO2015128582 (A1): 2017-01-04, 2015. https://patentscope.wipo.int/search/fr/detail.jsf?docId=WO2015128582 (accessed March 18, 2021).

[19] A. Barrera, C. Binet, F. Dubois, P.A. Hébert, P. Supiot, C. Foissac, U. Maschke, Dielectric spectroscopy analysis of liquid crystals recovered from end-of-life liquid crystal displays, Molecules. 26 (2021). https://doi.org/10.3390/molecules26102873.

[20] W.H.H. Woodward, Broadband Dielectric Spectroscopy - A Practical Guide, in: ACS Symposium Series (Ed.), Broadband Dielectr. Spectrosc. A Mod. Anal. Tech., 1 st, American Chemical Society, Washington, DC, United States, 2021: pp. 3–59. https://doi.org/10.1021/bk-2021-1375.ch001.

[21] A.K. Jonscher, The “universal” dielectric response, Nature. 267 (1977) 673–679. https://doi.org/https://doi.org/10.1038/267673a0.

[22] D.W. Davidson, R.H. Cole, Dielectric relaxation in glycerine, J. Chem. Phys. 18 (1950) 1417. https://doi.org/10.1063/1.1747496.

[23] K.S. Cole, R.H. Cole, Dispersion and absorption in dielectrics: II. Direct current characteristics, J. Chem. Phys. 10 (1942) 98–105. https://doi.org/10.1063/1.1723677.

[24] S. Havriliak, S. Negami, A complex plane representation of dielectric and mechanical relaxation processes in some polymers, Polymer (Guildf). 8 (1967) 161–210. https://doi.org/10.1016/0032-3861(67)90021-3.

[25] P. Pawel, H.M. Godinho, Liquid crystals. New perspectives, 1 st ed., John Wiley & Sons, Inc., Hoboken, NJ, USA, 2021.

[26] F. Kremer, A. Schönhals, Broadband dielectric spectroscopy, 1st ed, Springer-Verlag Berlin Heidelberg: New York, USA, 2003. http://books.google.com/books?id=sdG4ywL3qMsC.

[27] M.T. Viciosa, A.M. Nunes, A. Fernandes, P.L. Almeida, M.H. Godinho, M.D. Dionísio, Dielectric studies of the nematic mixture E7 on a hdroxypropylcellulose substrate, Liq. Cryst. 29 (2002) 429–441. https://doi.org/10.1080/02678290110113478.

[28] G. Yadav, R. Katiyar, G. Pathak, R. Manohar, Effect of ion trapping behavior of TiO2 nanoparticles on different parameters of weakly polar nematic liquid crystal, J. Theor. Appl. Phys. 12 (2018) 191–198. https://doi.org/10.1007/s40094-018-0296-x.

[29] P. Perkowski, D. Łada, K. Ogrodnik, J. Rutkowska, W. Piecek, Z. Raszewski, Technical aspects of dielectric spectroscopy measurements of liquid crystals, Opto-Electronics Rev. 16 (2008) 271–276. https://doi.org/10.2478/s11772-008-0008-1.

[30] R. Dhar, An impedance model to improve the higher frequency limit of electrical measurements on the capacitor cell made from electrodes of finite resistances, Indian J. Pure Appl. Phys. 42 (2004) 56–61.

[31] P. Perkowski, Dielectric spectroscopy of liquid crystals. Electrodes resistivity and connecting wires inductance influence on dielectric measurements, Opto-Electronics Rev. 20 (2012) 79–86. https://doi.org/10.2478/s11772−012−0004−3.

[32] P. Debye, Polar Molecules, 1st ed, Dover Publications, Inc., New York, USA, 1929. https://doi.org/10.1002/ANGE.19290424112.

[33] S. Krishna Prasad, M. Vijay Kumar, T. Shilpa, C.V. Yelamaggad, Enhancement of electrical conductivity, dielectric anisotropy and director relaxation frequency in composites of gold nanoparticle and a weakly polar nematic liquid crystal, RSC Adv. 4 (2014) 4453–4462. https://doi.org/10.1039/c3ra45761c.

[34] R.J. Mandle, E. Bevis, J.W. Goodby, Phase Structures of Nematic Liquid Crystals, in: J.W. Goodby, C. Tschierske, P. Raynes, H. Gleeson, T. Kato, P.J. Collings (Eds.), Handb. Liq. Cryst., 2 nd ed, Wiley-VCH Verlag GmbH & Co. KGaA., Weinheim, Germany, 2014: pp. 1–27. https://doi.org/10.1002/9783527671403.hlc037.